



1    **Heavy air pollution with the unique “non-stagnant”**  
2    **atmospheric boundary layer in the Yangtze River Middle**  
3    **Basin aggravated by regional transport of PM<sub>2.5</sub> over China**

4    Chao Yu<sup>1,2</sup>, Tianliang Zhao<sup>1,\*</sup>, Yongqing Bai<sup>3,\*</sup>, Lei Zhang<sup>1,4</sup>, Shaofei Kong<sup>5</sup>, Xingna Yu<sup>1</sup>, Jinhai  
5    He<sup>1</sup>, Chunguang Cui<sup>3</sup>, Jie Yang<sup>1</sup>, Yinchang You<sup>1</sup>, Guoxu Ma<sup>1</sup>, Ming Wu<sup>1</sup>, Jiacheng Chang<sup>1</sup>

6    1 Collaborative Innovation Center on Forecast and Evaluation of Meteorological Disasters, Key  
7    Laboratory for Aerosol-Cloud-Precipitation of China Meteorological Administration, Nanjing  
8    University of Information Science and Technology, Nanjing 210044, China

9    2 Southwest Electric Power Design Institute Co., Ltd of China Power Engineering Consulting  
10    Group, Chengdu, 610021, China

11    3 Institute of Heavy Rain, China Meteorological Administration, Wuhan, 430205, China

12    4 Chengdu Academy of Environmental Sciences, Chengdu, 610031, China

13    5 Department of Atmospheric Sciences, School of Environmental Studies, China University of  
14    Geosciences (Wuhan), 430074, Wuhan, China

15    *Correspondence:* Tianliang Zhao ([tlzhao@nuist.edu.cn](mailto:tlzhao@nuist.edu.cn)); Yongqing Bai (2007byq@163.com)

16

17    **Abstract:** Regional transport of air pollutants controlled by both emission sources and  
18    meteorological factors results in a complex source-receptor relationship of air pollution change.

19    Wuhan, a metropolis in the Yangtze River Middle Basin (YRMB) of central China experienced



20 heavy air pollution characterized by excessive  $\text{PM}_{2.5}$  concentrations reaching  $471.1 \mu\text{g m}^{-3}$  in  
21 January 2016. In order to investigate the regional transport of  $\text{PM}_{2.5}$  over China and the  
22 meteorological impact on wintertime air pollution in the YRMB area, observational  
23 meteorological and other relevant environmental data from January 2016 were analyzed. Our  
24 analysis presented the noteworthy cases of heavy  $\text{PM}_{2.5}$  pollution in the YRMB area with the  
25 unique “non-stagnant” meteorological conditions of strong northerly winds, no temperature  
26 inversion and additional unstable structures in the atmospheric boundary layer. This unique set of  
27 conditions differed from the stagnant meteorological conditions characterized by near-surface  
28 weak winds, air temperature inversion, and stable structure in the boundary layer observed in  
29 heavy air pollution over most regions in China. The regional transport of  $\text{PM}_{2.5}$  over  
30 central-eastern China aggravated  $\text{PM}_{2.5}$  levels present in the YRMB area, thus demonstrating the  
31 source-receptor relationship between the originating air pollution regions in central-eastern China  
32 and the receiving YRMB regions. Furthermore, a backward trajectory simulation using  
33 FLEXPART-WRF to integrate the air pollutant emission inventory over China was used to explore  
34 the patterns of regional transport of  $\text{PM}_{2.5}$  governed by the strong northerly winds in the cold air  
35 activity of the East Asian winter monsoon over central-eastern China, which contributes markedly  
36 to the heavy  $\text{PM}_{2.5}$  pollution in the YRMB area. It was estimated that the regional transport of  
37  $\text{PM}_{2.5}$  of non-local air pollutant emissions could contribute more than 65% of the  $\text{PM}_{2.5}$   
38 concentrations to the heavy air pollution in the YRMB region during the study period, revealing  
39 the importance of the regional transport of air pollutants over central-eastern China in the  
40 formation of heavy air pollution over the YRMB region.

41 **Key words:**  $\text{PM}_{2.5}$  pollution; Yangtze River Middle Basin; meteorological condition; regional



42 transport; FLEXPART-WRF

43

## 44 1. Introduction

45 Air pollution events with excessive ambient  $PM_{2.5}$  concentrations have been observed  
46 frequently in the central-eastern regions of China in recent years. These events result in serious  
47 environmental problems with adverse influence on traffic, human health, climate change and other  
48 significant aspects (Fuzzi et al., 2015; An et al., 2019; Nel, 2005). Based on the observations in  
49 China, there is a well-established association between haze pollution and high concentrations of  
50  $PM_{2.5}$  (particulate matter with an aerodynamical diameter less than  $2.5\ \mu m$ ). Air pollution levels  
51 are highly dependent on emissions of air pollutants and changes in meteorology (Tie et al., 2017;  
52 Xu et al., 2016b; An et al., 2019; Xu et al., 2016a). The accumulation, maintenance and dissipation  
53 of haze pollution events are generally determined by meteorological changes (Kan et al., 2012),  
54 among which the boundary layer structures play the most important role (Wu et al., 2017).  
55 Meteorological conditions of stagnation characterized by near-surface low winds, high humidity  
56 and stable boundary layer could govern the periodic variations of haze pollution, which present as  
57 typical wintertime air pollution in central-eastern China (Xu et al., 2016b; Zhang et al., 2014;  
58 Huang et al., 2018). Four major regions exhibiting haze pollution with high  $PM_{2.5}$  concentrations  
59 and overall poor air quality are centered over North China Plain (NCP), Yangtze River Delta  
60 (YRD) in East China, Pearl River Delta (PRD) in South China and Sichuan Basin (SCB) in  
61 Southwest China (Cheng et al., 2008; Zhang et al., 2012; Deng et al., 2011; Wang et al., 2016; Tie  
62 et al., 2017; Qiao et al., 2019).



63        The source-receptor relationship describes the impacts of emissions from an upwind source  
64        region to pollutant concentrations or deposition at a downwind receptor location.    Regional  
65        transport of source-receptor air pollutants is generally complicated by two types of    factors:  
66        emission and meteorology. The emission factor includes the emission source strength, chemical  
67        transformation and production; the meteorological factor determines the transport pathway from  
68        the source to receptor regions, exchanges between boundary layer and free troposphere, the  
69        removal processes occurring over the source and receptor regions as well as along the transport  
70        pathways. Regional transport of air pollutants with the source-receptor relationship is an important  
71        issue in our understanding of changes in air quality. Driven by atmospheric circulation, the  
72        regional transport of  $PM_{2.5}$  from source regions can deteriorate air quality in the downwind  
73        receptor regions, leading to the regional haze pollution observed in a large area over  
74        central-eastern China (Chang et al., 2018; Wang et al., 2014; He et al., 2017; Chen et al., 2017b;  
75        Hu et al., 2018; Jiang et al., 2015). The Yangtze River Middle Basin (YRMB) in central China is  
76        geographically surrounded by four major haze pollution regions in all directions with NCP to the  
77        north, the YRD to the east, the PRD to the south and the SCB to the west (Fig.1 a). Due to this  
78        specialized location of the YRMB as a regional air pollutant transport hub with subbasin  
79        topography (see Fig. 1b), the regional transport of air pollutants driven by the cold air activity of  
80        East Asian winter monsoonal winds in central-eastern China could develop a source-receptor  
81        relationship between major haze pollution regions (NCP, YRD, etc.) in central-eastern China and  
82        the downwind YRMB region. However, there are unresolved questions regarding the  
83        meteorological processes involved in the regional transport of air pollutants    and the pattern of  
84        regional transport with contribution to the air quality changes observed in the YRMB.



85 Wuhan, a metropolis located in the YRMB, has confronted the problems associated with urban air  
86 pollution, especially heavy  $\text{PM}_{2.5}$  pollution events that occur in the winter (Zhong et al., 2014;  
87 Gong et al., 2015; Xu et al., 2017; Tan et al., 2015). Local emissions of air pollutants from urban  
88 transportation, industrial exhaust and bio-combustion play an important role in YRMB urban air  
89 pollution (Acciai et al., 2017; Zhang et al., 2015). Many observational and modeling studies on air  
90 pollution in this urban area have been conducted (Zheng et al., 2019; Wu et al., 2018). However,  
91 regional transport routes of  $\text{PM}_{2.5}$  from central-eastern China and its contribution to air pollution  
92 over the YRMB are still poorly understood, especially in relation to heavy air pollution episodes in  
93 the YRMB area. This study selected the Wuhan area as a representative area within the YRMB for  
94 investigation of the meteorological conditions of air pollution events in January 2016 and the  
95 contribution of regional transport of  $\text{PM}_{2.5}$  to heavy air pollution over the YRMB region.

## 96 **2. Observational analysis**

### 97 **2.1 Data**

98 Wuhan, the capital of Hubei province, is located across the Yangtze River, where its surrounding  
99 water network attributed with a humid environment. (see Fig. 1b). In order to analyze the air  
100 quality change, the hourly concentrations of air pollutants including  $\text{PM}_{2.5}$  in January 2016 were  
101 collected from sites over central-eastern China, including ten observational sites in Wuhan. These  
102 ten sites include nine urban sites in residential and industrial zones as well as one suburban site  
103 within the China National Air Environmental Monitoring Network. The concentrations of air  
104 pollutants were distributed spatially in less difference over the suburban and urban sites with the  
105 similar patterns and peaks of hourly changes during the heavy pollution events, demonstrating the



106 regional heavy air pollution in a large area of the YRMB region with the contribution of regional  
107 transport from central-eastern China, while the obviously differences in air pollutant  
108 concentrations were measured with the relative high and low  $PM_{2.5}$  concentrations respectively at  
109 urban sites and suburban site during the clean air period, reflecting the important influence of high  
110 air pollutant emission over urban area on local air quality. The  $PM_{2.5}$  concentrations averaged over  
111 the ten observational sites were used to characterize the variations of air pollution in January 2016  
112 over this urban area within the YRMB.

113 The meteorological data of surface observation and air sounding in Wuhan and other  
114 observatories in central-eastern China were obtained from the China Meteorological Data Sharing  
115 Network (<http://data.cma.cn/>). Meteorological data selected for this study included horizontal  
116 visibility, air temperature, relative humidity, air pressure, and wind speed and direction with  
117 temporal resolutions of 3 h for surface observation and 12 h for sounding observation in order to  
118 analyze the variations of the meteorological conditions in the atmospheric boundary layer in  
119 January 2016.

120 The ERA (ECMWF ReAnalysis) -Interim reanalysis data of meteorology from the  
121 ECMWF (European Centre for Medium-Range Weather Forecasts)  
122 (<https://www.ecmwf.int/en/forecasts/datasets/reanalysis-datasets/>) were applied to explore the cold  
123 air activity of East Asian winter monsoonal winds in January 2016 and their anomalies during  
124 heavy  $PM_{2.5}$  pollution the over central-eastern China .

## 125 **2.2 Variations in $PM_{2.5}$ concentrations and meteorology in January, 2016**

126 Based on the National Ambient Air Quality Standards of China released by the Ministry of



Ecology and Environment of China in 2012 (<http://www.mee.gov.cn/>), light and heavy air pollution levels of  $\text{PM}_{2.5}$  are categorized by daily average  $\text{PM}_{2.5}$  concentration exceeding  $75\mu\text{g m}^{-3}$  and  $150\mu\text{g m}^{-3}$  in ambient air, respectively. The daily variations of  $\text{PM}_{2.5}$  concentrations over January 2016 in Wuhan are illustrated in Figure 2a. The average monthly  $\text{PM}_{2.5}$  concentration reached  $105.8\mu\text{g m}^{-3}$ . The national secondary standard was exceeded on 27 days with daily  $\text{PM}_{2.5}$  concentrations exceeding  $75\mu\text{g m}^{-3}$  during the entire month of January 2016 in Wuhan, indicating that this urban area in the YRMB was suffering under significant  $\text{PM}_{2.5}$  pollution during this period. As shown in Figure 2a, a 21-day prolonged air pollution event resulted from high levels of daily  $\text{PM}_{2.5}$  concentrations ( $>75\mu\text{g m}^{-3}$ ) over the period of January 1 to 21. During this 21-day period of air pollution, three notably heavy air pollution events occurred on January 4, 10-12 and 18 with excessive daily  $\text{PM}_{2.5}$  concentrations ( $>150\mu\text{g m}^{-3}$ ); these events are marked as P1, P2 and P3 in Figure 2. Based on the observation in January 2016, we found the interesting phenomenon of an apparent 7-day cycle of heavy air pollution in January 2016, reflecting an important modulation of meteorological oscillation in the East Asian winter monsoon affecting air pollution concentrations observed over the YRMB region (Xu et al., 2016a). A period analysis on long-term observation data of air quality could provide more information on air pollution oscillations with meteorological drivers.

Figure 2b presents the hourly changes of  $\text{PM}_{2.5}$  concentrations for the three heavy air pollution events P1, P2 and P3. The heavy pollution event P1 on January 4 started at 11:00 am (local time is used for all events) and ended at 11:00 pm at same day. with an observed  $\text{PM}_{2.5}$  concentration peak of  $471.1\mu\text{g m}^{-3}$ . The event P2 occurred from 10:00 pm on January 10 to 00:00 a.m. on January 12 with a duration of 26 h and two peaks in  $\text{PM}_{2.5}$  concentrations of  $231.4\mu\text{g m}^{-3}$  and  $210.6\mu\text{g m}^{-3}$ .



149 The event P3 was observed between 7:00 p.m. on January 17 and 2:00 pm on January 18 with an  
150 explosive growth rate of  $42.9\mu\text{g m}^{-3}\text{h}^{-1}$  in  $\text{PM}_{2.5}$  concentrations. Those three heavy  $\text{PM}_{2.5}$  pollution  
151 episodes over the YRMB region were characterized by short durations of less than 26 h from rapid  
152 accumulation to fast dissipation.

153 Using the environmental and meteorological data observed in Wuhan in January 2016, the effects  
154 of the meteorological conditions on  $\text{PM}_{2.5}$  concentrations in the YRMB region were statistically  
155 analyzed in regards to hourly variations of surface  $\text{PM}_{2.5}$  concentrations, near-surface wind speed  
156 (WS) and direction (WD), as well as surface air temperature (T), air pressure (P) and relative  
157 humidity (RH) (Fig. 3). Among the observed hourly changes in  $\text{PM}_{2.5}$  concentrations and  
158 meteorological elements shown in Figure 3, the obvious positive correlations to surface air  
159 temperature and relative humidity, as well as a pronounced negative correlation to surface air  
160 pressure and a weak positive correlation to near-surface wind speed were found with the change of  
161  $\text{PM}_{2.5}$  concentrations in January 2016 (Table 1). The near-surface wind speed associated with East  
162 Asian monsoons has significantly influence concentrations of air pollutants mainly by the changes  
163 in weak advection of cold air, in conjunction with strong subsidence and stable atmospheric  
164 stratification, can easily produce a stagnation area in the lower troposphere resulting in regional  
165 pollutant accumulations, which are favorable for the development of CEC haze events. In addition,  
166 in the presence of high soil moisture, strong surface evaporation results in increases in the  
167 near-surface relative humidity, which is also conducive to hygroscopic growth of particles for  
168 haze formation; high air temperature and strong solar radiation could enhance chemical reactions  
169 and conversions for the formation of secondary aerosols in the atmosphere, precipitation could  
170 alter the emissions, and depositions of air pollutants. These observations could reflect the special





171 influences of meteorological factors (winds, air temperature, humidity, precipitation etc) on  
172 physical and chemical processes in the ambient atmosphere, in particular that of wind driving air  
173 pollutant transport and affecting air quality change in the YRMB region.

174       When we focused on the changes leading to excessive  $PM_{2.5}$  levels during these heavy air  
175 pollution events, it is noteworthy that all three heavy pollution episodes P1, P2 and P3 were  
176 accompanied with strong near-surface wind speeds in the northerly direction, as well as evident  
177 turning points in prevailing conditions leading to falling surface air temperatures and increasing  
178 surface air pressure (noted as a rectangle with red dashed lines in Fig. 3). The conditions observed  
179 during these three heavy pollution episodes reflect the typical meteorological characteristics of  
180 cold front activity over the East Asian monsoon region. The southward advance of a cold front  
181 could drive the regional transport of air pollutants over central-eastern China (Kang et al., 2019).  
182 Climatologically, a strong northerly wind, low air temperature and high air pressure are typical  
183 features of an incursion of cold air during East Asian winter monsoon season in central-eastern  
184 China, which could disperse air pollutants and improve air quality in the NCP region (Miao et al.,  
185 2018; Xu et al., 2016b). Compared to the meteorological conditions for stagnation with weak  
186 winds observed for heavy air pollution events in the major air pollution regions of central-eastern  
187 China (Huang et al., 2018; Ding et al., 2017), meteorological conditions with strong near-surface  
188 wind were anomalously accompanied with the intensification of  $PM_{2.5}$  during heavy air pollution  
189 periods over the study area in the YRMB in January 2016 (Fig. 3). This could imply the  
190 importance of regional air pollutant transport in worsening air quality over the YRMB, driven by  
191 the strong northerly winds of the East Asian winter monsoon over China.



## 192    **2.3 A unique “non-stagnation” meteorological condition for heavy PM<sub>2.5</sub>** 193    **pollution**

194    To further investigate the connection of meteorological elements in the near-surface layer with  
195    changes in air quality affected by PM<sub>2.5</sub> concentrations in the YRMB region, we carried out a more  
196    detailed correlation analysis of PM<sub>2.5</sub> concentrations in Wuhan with near-surface wind speed and  
197    air temperature and three different levels of PM<sub>2.5</sub> concentrations: clean air environment  
198    (PM<sub>2.5</sub> < 75 μg m<sup>-3</sup>), light air pollution (75 μg m<sup>-3</sup> ≤ PM<sub>2.5</sub> < 150 μg m<sup>-3</sup>) and heavy air pollution (PM<sub>2.5</sub>  
199    ≥ 150 μg m<sup>-3</sup>) periods (Table 2). As seen in Table 2, the surface PM<sub>2.5</sub> concentrations were  
200    positively correlated with air temperature, as well as negatively correlated with wind speeds  
201    during the periods of clean air environment and light air pollution. It should be emphasized here  
202    that a significantly negative correlation (R = -0.19) of PM<sub>2.5</sub> concentrations with near-surface wind  
203    speeds for the light air pollution period could indicate that weak winds are favorable for local  
204    PM<sub>2.5</sub> accumulation, reflecting an important effect of local air pollutant emissions on light air  
205    pollution periods over the YRMB area. In January 2016, the overall wind speed of Wuhan was  
206    weak with a monthly mean value of 2.0 m s<sup>-1</sup>, which could prove beneficial to maintaining the high  
207    PM<sub>2.5</sub> levels in the prolonged air pollution event experienced during January 2016. However, a  
208    significantly positive correlation (R = 0.41) existed between excessive PM<sub>2.5</sub> concentrations  
209    (PM<sub>2.5</sub> > 150 μg m<sup>-3</sup>) and strong near-surface wind speeds during the heavy air pollution period,  
210    which was inconsistent with the stagnation meteorological conditions observed in the near-surface  
211    layer with weak winds associated with heavy air pollution in eastern China (Cao et al., 2012;  
212    Zhang et al., 2016). The meteorology and environment conditions in the YRMB region indicate  
213    the close association of heavy air pollution periods with the intensification of regional transport of



214 air pollutants driven by strong winds (Fig. 3, Table 2) reflecting a key role of regional air pollutant  
215 transport in the development of the YRMB's heavy air pollution periods.

216 In order to clearly illustrate the impact of wind speed and direction on the  $PM_{2.5}$  concentrations  
217 associated with the regional transport of upwind air pollutants, Figure 4 presents the relation of  
218 hourly changes in surface  $PM_{2.5}$  concentrations (in color contours) to near-surface wind speed (in  
219 radius of round) and direction (in angles of round) in Wuhan during January 2016. As can be seen  
220 in Figure 4, strong northerly winds of the East Asian winter monsoon accompanied extremely high  
221  $PM_{2.5}$  concentrations ( $>150\mu g\ m^{-3}$ ) during heavy air pollution periods, including the northeast gale  
222 that exceeded  $5\ m\ s^{-1}$  during the extreme heavy pollution period with excessive high  $PM_{2.5}$   
223 concentrations ( $>300\mu g\ m^{-3}$ ) over the YRMB region. These results reveal a unique meteorological  
224 condition of “non-stagnation” with strong winds during events of heavy air pollution over YRMB  
225 area. Conversely, the observed  $PM_{2.5}$  concentrations ranging between 75 and  $150\mu g\ m^{-3}$  for light  
226 air pollution periods generally corresponded with low wind speed ( $<2\ m\ s^{-1}$ ) in the YRMB region  
227 (Fig. 4); therefore, it is the meteorological condition for stagnation characterized by weak winds  
228 involved in the accumulation of local air pollutants that is responsible for the YRMB's light air  
229 pollution periods. Meteorological impacts on air quality could include not only the stagnation  
230 condition with weak winds and stable boundary layer, but also air temperature, humidity,  
231 precipitation, atmospheric radiation etc. in close connection with atmospheric physical and  
232 chemical processes. Therefore, meteorological drivers of air quality change are complicated by a  
233 series of physical and chemical processes in the atmosphere especially the formation of secondary  
234 air pollutants in the humid air environment overlying the dense water network in the YRMB  
235 region (see Fig. 1b), thus pointing out the need for further comprehensive study.



236 As shown in Figure 2a, the heavy pollution periods with the daily average  $PM_{2.5}$   
237 concentrations exceeding  $150\mu g m^{-3}$  in ambient air, respectively occurred on January 4, 10-12 and  
238 18, and the clean air periods with the daily average  $PM_{2.5}$  concentrations below  $75\mu g m^{-3}$  occurred  
239 on January 22 and 24-27, 2016, in the YRMB region. The air sounding data of Wuhan were used  
240 to compare the structures of the atmospheric boundary layer of the heavy air pollution and clean  
241 air periods. Figure 5 presents the vertical profiles of air temperature, wind velocity and potential  
242 temperature averaged for the heavy  $PM_{2.5}$  pollution and clean air periods in January 2016. It can  
243 be clearly seen that the inversion layer of air temperature did not exist during the heavy pollution  
244 periods, but a near-surface inversion layer appeared at the height of about 200 m during the clean  
245 air periods (Fig. 5a). The comparison of vertical profiles of horizontal wind velocity experienced  
246 during the clean air periods further revealed the stronger wind speed observed in the heavy air  
247 pollution period below a height of 850 m located in the atmospheric boundary layer exhibiting the  
248 vertical structure similar to a low-level jet stream (Fig. 5b); these conditions could conduce the  
249 downward mixing of the regionally transported air pollutants and produce a local near-surface  
250 accumulation in the YRMB area with elevated ambient  $PM_{2.5}$  concentrations, thus contributing to  
251 a heavy air pollution. To characterize the atmospheric stability in the boundary layer, the vertical  
252 profiles of potential air temperature ( $\theta$ ) were calculated with air temperature and pressure (Fig. 5c).  
253 The vertical change rate of  $\theta$  was used to quantify the static stability of the boundary layer in this  
254 study (Oke, 2002; Sheng et al., 2003). A lower vertical change rate of  $\theta$  generally indicates a  
255 decreasing stability or increasing instability of the boundary layer. The averaged static stability  
256 values of the near-surface layer below a height of 200 m during the heavy pollution and clean air  
257 periods were approximately  $4.4K \cdot km^{-1}$  and  $13.2K \cdot km^{-1}$ , respectively (Table 3). This obvious



258 decrease in stability of the boundary layer from clean air to heavy pollution periods reflects an  
259 anomalous tendency for instability in the boundary layer during heavy pollution periods in the  
260 YRMB region during January 2016.

261 The meteorological conditions of stagnation characterized by weak wind, temperature  
262 inversion and a stable vertical structure of the atmospheric boundary layer is generally accepted as  
263 the typical meteorological drivers for heavy air pollution (An et al., 2019; Ding et al., 2017).  
264 Nevertheless, this study of environmental and meteorological observations in the YRMB region  
265 has revealed a unique meteorological condition of “non-stagnation” in the atmospheric boundary  
266 layer during heavy air pollution periods characterized by strong wind, lack of an inversion layer  
267 and a more unstable structure of the atmospheric boundary layer; these conditions are generally  
268 regarded as the typical pattern of atmospheric circulation that facilitates the regional transport of  
269 air pollutants from upstream source to downwind receptor regions. Regional transport of PM<sub>2.5</sub>  
270 associated with the source-receptor relationship between the air pollution regions in  
271 central-eastern China and the YRMB was investigated based on the observational analysis  
272 described in Sect. 3.1.

### 273 **3. Regional transport of PM<sub>2.5</sub> in heavy air pollution periods**

#### 274 **3.1 Changes of PM<sub>2.5</sub> and winds observed in central-eastern China**

275 The monthly averages of observed PM<sub>2.5</sub> concentrations and the anomalies of wind speed  
276 averaged in three heavy air pollution periods relatively to the monthly mean wind speed in January  
277 2016 over central-eastern China are shown in Figure 6. In January 2016, a large area of  
278 central-eastern China experienced air pollution with high levels of PM<sub>2.5</sub> (>75 µg m<sup>-3</sup>), especially



serious in the NCP region and the Fenhe-Weihe Plain in central China (Fig. 6a). As seen in Figure 6, the YRMB region (Site 1, Wuhan) was situated in the downwind southern edge of an observed air pollution area located over central-eastern China, where the northerly winds of the East Asian winter monsoon prevail climatologically in January (Ding, 1994). It is notable that the anomalously stronger northerly winds were observed over the upstream region in central-eastern China during three periods of wintertime heavy  $PM_{2.5}$  pollution in the YRMB region (Fig. 6b). Driven by the strong northerly winter monsoonal winds (Fig. 6b), the regional transport of air pollutants from the source regions in central-eastern China could largely contribute to wintertime heavy air pollution periods in the downwind receptor region of YRMB.

In order to explore the connection of regional transport of  $PM_{2.5}$  over central-eastern China to three events of heavy air pollution in the YRMB region, six observational sites were selected from the northwestern, northern and northeastern upwind areas located over central-eastern China (Fig. 6a) to represent the temporal  $PM_{2.5}$  and wind variations along the different routes of regional transport of  $PM_{2.5}$  with the southward incursion of stronger northerly winds of East Asian monsoon across central-eastern China (Fig. 7). The southeastward movement of heavy  $PM_{2.5}$  pollution driven by stronger northerly winds from Luoyang and Xinyang to Wuhan (Sites 3, 2, and 1 in Fig. 6) presents a northwestern route of regional transport of  $PM_{2.5}$  for the heavy air pollution period P1 in the YRMB (see upper panels of Fig. 7). The southwestward advance of  $PM_{2.5}$  peaks governed by winter monsoonal winds from Tongling and Hefei to Wuhan (Sites 5, 6, and 1 in Fig. 6) exerted a significant impact on the heavy air pollution period P2 aggravated by regional transport of  $PM_{2.5}$  across Eastern China to the YRMB region (see middle panels of Fig. 7). A northern pathway of regional transport of  $PM_{2.5}$  connected Zhengzhou and Xinyang to Wuhan



301 (Sites 4, 2, and 1 in Fig. 6) during the YRMB's heavy air pollution period P3 with anomalously  
302 strong northerly winds (see Fig. 6b and lower panels of Fig. 7). It is noteworthy in Fig. 7 that the  
303 heavy PM<sub>2.5</sub> pollution periods at the upstream sites Hefei, Tongling, Luoyang, Xinyang and  
304 Zhengzhou (Fig. 6a) were generally dispelled by strong northerly winds, while strong northerly  
305 winds could trigger the periods of heavy PM<sub>2.5</sub> pollution in the YRMB region (Wuhan, Fig. 6), and  
306 such inverse effects of strong winds on heavy air pollution in the source and receptor regions  
307 reflect an important role of regional air pollutant transport in worsening air pollution in the  
308 YRMB's receptor region.

309 The regional transport over central-eastern China associated with the source-receptor  
310 relationship directing heavy PM<sub>2.5</sub> pollution to the YRMB region was revealed with observational  
311 analysis. Backward trajectory modeling was used to further confirm the patterns of regional  
312 transport of PM<sub>2.5</sub> over central-eastern China and the resulting contribution to heavy air pollution  
313 in the YRMB region, as described in the following Sects.

### 314 **3.2 FLEXPART-WRF model**

#### 315 3.2.1 Model description

316 The Flexible Particle dispersion (FLEXPART) model (Stohl, 2003) is a Lagrange particle  
317 diffusion model developed by the Norwegian Institute for Air Research (NIAR). In this model, the  
318 trajectory of a large number of particles released from a source is simulated with consideration of  
319 the processes of tracer transport, turbulent diffusion, and wet and dry depositions in the  
320 atmosphere (Brioude et al., 2013). Applying backward trajectory simulation can determine the  
321 distribution of potential source regions that may have an impact on a target point or receptor



322 region (Seibert and Frank, 2003; Zhai et al., 2016; Chen et al., 2017a; Chen et al., 2017b).

323 Initially, FLEXPART could be driven by the global reanalysis meteorological data obtained  
324 from the European Centre for Medium-Range Weather Forecasts (ECMWF) or the National  
325 Centers of Environmental Prediction (NCEP). For the refined simulation of air pollutant sources  
326 and transport, FLEXPART was coupled offline with the Weather Research and Forecasting Model  
327 (WRF) to effectively devise the combined model FLEXPART-WRF (Fast and Easter, 2006), which  
328 has been widely used to investigate the potential sources of air pollutants in consideration of  
329 environmental change (Stohl, 2003; De Foy et al., 2011; An et al., 2014; Sauvage et al., 2017).

### 330 3.2.2 Model configuration

331 The WRF model was configured with two nested domains. The coarse domain covered the  
332 entirety of Asia with a 30 km×30 km horizontal resolution, and the nested fine domain included  
333 most of China and surrounding regions with a 10 km×10 km horizontal resolution. The physical  
334 parameterizations used in WRF were selected with the Morrison microphysics scheme (Morrison,  
335 2009), the Rapid Radiative Transfer Model (RRTM) scheme for long and short wave radiation  
336 (Mlawer et al., 1997), the Yonsei University (YSU) boundary layer scheme (Hong, 2006), Grell  
337 3D cumulus parameterization, and the Noah land surface scheme (Grell et al., 2005). Driven with  
338 the reanalysis meteorological data obtained from NCEP for initial and boundary meteorological  
339 conditions, the WRF simulation ran 12 h each time with the first 6 h simulations constituting  
340 spin-up time.

341 The FLEXPART-WRF simulation was conducted for the 48-hr backward trajectory with a  
342 release of 50,000 PM<sub>2.5</sub> particles per hour in Wuhan (30.61N, 114.42E) for January 2016. The





343 48-hr backward trajectory simulation results were output with the residence time of  $\text{PM}_{2.5}$  particles  
344 in a horizontally resolution of  $0.1^\circ \times 0.1^\circ$ . The FLEXPART simulations of  $\text{PM}_{2.5}$  particle residence  
345 time over the 48-hr backward trajectory pathways were multiplied with the regional primary  $\text{PM}_{2.5}$   
346 emission fluxes to quantify the contribution of regional transport of  $\text{PM}_{2.5}$  to air quality change in  
347 the YRMB region with identifying the patterns of regional transport of  $\text{PM}_{2.5}$  over central-eastern  
348 China. The primary  $\text{PM}_{2.5}$  emission data of 2016 obtained from the Multi-resolution Emission  
349 Inventory for China (MEIC, <http://www.meicmodel.org/>) were selected for use as the regional  
350  $\text{PM}_{2.5}$  emission fluxes in this study.

### 351 3.2.3 Validation of modeling results

352 The simulated meteorology, which included wind speed, air temperature, relative humidity  
353 and surface pressure, were compared with observations at five sites (Wuhan, Changsha, Hefei,  
354 Zhengzhou and Nanchang) over central-eastern China. The correlation coefficients and  
355 normalized standardized deviations were calculated and are shown in Figure 8 (Taylor, 2001).  
356 Based on the results with correlation coefficients passing the significance level of 0.001 and low  
357 normalized standardized deviations (Fig. 8), it was confirmed that WRF-modeled meteorology  
358 that is consistent with observations could be used to drive the FLEXPART backward trajectory  
359 simulation in this study.

### 360 3.3 Contribution of regional transport of $\text{PM}_{2.5}$ to heavy pollution

361 Based on the FLEXPART-WRF backward trajectory simulation, the upstream sources of  
362  $\text{PM}_{2.5}$  emissions for heavy air pollution in Wuhan could be identified. The contribution rates *rate<sub>ij</sub>*  
363 of regional transport of  $\text{PM}_{2.5}$  from the upstream sources to air pollution in the downstream



receptor region of YRMB were calculated by Eq. (1), and the total contribution  $R$  of regional transport from the non-local emission sources are estimated by Eq. (2) (Chen et al., 2017b).

$$rate_{i,j} = \frac{E_{i,j} \times r_{i,j}}{\sum_{i=1}^{N,S} E_{i,j} \times r_{i,j}} \quad (1)$$

$$R = \sum_{(N_1, S_1)}^{(N_2, S_2)} rate_{i,j} \quad (2)$$

where the subscripts  $i$  and  $j$  represent a grid location;  $r_{i,j}$  represents the residence time of  $PM_{2.5}$  particles simulated by FLEXPART-WRF; and,  $E_{i,j}$  represents the  $PM_{2.5}$  emission flux over the grid. The first grid location ( $N_1, S_1$ ) and the last grid location ( $N_2, S_2$ ) over the non-local emission sources and the local area of Wuhan were determined respectively by the regional transport of  $PM_{2.5}$  pathways and the YRMB region as simulated by FLEXPART-WRF.

The non-local emission sources that affected  $PM_{2.5}$  concentrations during three heavy pollution periods through regional transport to the YRMB region were quantified by calculation of the  $PM_{2.5}$  contribution rates with Eq (1). Combining the distribution of high  $PM_{2.5}$  contribution rates with the prevailing winds experienced during the three heavy  $PM_{2.5}$  pollution periods, the spatial distribution of the major pathways of regional transport of  $PM_{2.5}$  over central-eastern China could be recognized as shown in Figure 9. During the heavy air pollution period P1 in the YRMB region, the regional transport of air pollutants was centered along a northwestern route from the Fenhe-Weihe Plain in central China and a northeastern route from the YRD region (Fig. 9a). The YRD emission sources of air pollutants in East China exerted an important impact on the heavy air pollution period P2 through regional transport of  $PM_{2.5}$  cross East China to the YRMB region along the north side of Yangtze River (Fig. 9b). Two major regional transport pathways of  $PM_{2.5}$  indicated by the spatial distribution of high contribution rates of  $PM_{2.5}$  from the NCP and YRD



regions respectively to the elevated  $PM_{2.5}$  concentrations during the YRMB's heavy air pollution period P3 (Fig. 9c). Governed by the northerly winds of the East Asian winter monsoon, the regional transport of air pollutants from the central-eastern air pollutant emission source regions in China provided a significant contribution to the wintertime heavy  $PM_{2.5}$  pollution observed in the YRMB region (Figs. 6-7), which was confirmed by the results of the FLEXPART-WRF backward trajectory simulation utilized in this study.

In this study, the  $PM_{2.5}$  contributions of regional transport to air pollution in the downwind receptor region could be approximately estimated based on the product of the residence time of  $PM_{2.5}$  particles during regional transport simulated by FLEXPART-WRF, and the  $PM_{2.5}$  emission flux over the source grid. The  $PM_{2.5}$  contributions of regional transport over central-eastern China to  $PM_{2.5}$  concentrations during three heavy  $PM_{2.5}$  pollution periods P1, P2 and P3 in the YRMB region were estimated using Eq. (2) with resulting high contribution rates of 68.1%, 60.9% and 65.3%, respectively (Table 4), revealing the significant contribution of regional transport of  $PM_{2.5}$  over central-eastern China to the enhancement of  $PM_{2.5}$  levels in the YRMB area during wintertime heavy air pollution periods.

Normally people rely on 3-D numerical models with process analysis capability such as integrated process rates (IPRs) to quantify the contributions of regional transport to the occurrence of air pollution episodes. It should be pointed out that the simulations with a Lagrange particle dispersion model FLEXPART-WRF are utilized to calculate the percentage contribution of regional transport with identifying the transport pathway in this study. The major uncertainty of this method for such calculation as compared to other methods like IPRs is that the physical and chemical processes such as wet-deposition and chemical conversion for the formation of



secondary particles are not introduced in the FLEXPART-WRF simulation, which could represent the basic features of contribution and patterns of regional transport of  $PM_{2.5}$  over central-eastern China when limited to the primary  $PM_{2.5}$  particles highlighted in this study.

#### 4. Conclusions

This study investigated the ambient  $PM_{2.5}$  variations over Wuhan, a typical urban YRMB region in central-eastern China in January 2016 through analysis of observational data of environment and meteorology, as well as via FLEXPART-WRF simulation to explore 1) the meteorological processes involved in the regional transport of air pollutants and 2) regional transport patterns of  $PM_{2.5}$  with the contribution to the air pollution in the YRMB region. Based on observation and simulation studies on the meteorological conditions of air pollution events in January 2016 and regional transport of  $PM_{2.5}$  to heavy air pollution over the YRMB region, it is revealed heavy air pollution with the unique “non-stagnant” atmospheric boundary layer in the YRMB region aggravated by regional transport of  $PM_{2.5}$  over central and eastern China.

The study of the effects of meteorology and regional transport of  $PM_{2.5}$  on heavy air pollution were focused on three heavy  $PM_{2.5}$  pollution periods in January 2016. The heavy pollution episodes observed with the peak of  $PM_{2.5}$  concentrations exceeding  $471\mu g\ m^{-3}$  over the YRMB region were characterized by a short duration of less than 26 hr from rapid outbreak to fast dissipation.

The “stagnation” meteorological condition in the boundary layer characterized by weak wind, air temperature inversion and a stable vertical structure of the atmospheric boundary layer is currently accepted as a typical meteorological driver for heavy air pollution. Conversely, this study



427 of environmental and meteorological observations in the YRMB region revealed a unique  
428 “non-stagnation” meteorological condition of the boundary layer characterized by strong wind, no  
429 inversion layer and a more unstable structure in the atmospheric boundary layer associated with  
430 heavy air pollution periods with excessive  $PM_{2.5}$  concentrations in the YRMB region, which  
431 facilitates understanding of the air pollutant source-receptor relationship of regional air pollutant  
432 transport.

433 Although the emissions and local accumulation of air pollutants in the YRMB could lead to  
434 the formation of light air pollution, in regards to  $PM_{2.5}$ , over the YRMB region, the regional  
435 transport of  $PM_{2.5}$  from central-eastern emission source regions in China contributed significantly  
436 to 65% of the exceedances of  $PM_{2.5}$  concentrations during wintertime heavy air pollution periods  
437 in the downwind YRMB region in January 2016, as governed by the strong northerly winds of the  
438 East Asian winter monsoon.

439 Based on the variations of air quality and meteorology in a typical urban YRMB region in  
440 January 2016, this study revealed a unique “non-stagnant” meteorological condition for the  
441 development of heavy air pollution in the YRMB region with strong contributions of regional  
442 transport of  $PM_{2.5}$  over central-eastern China. These conditions and contributions can be  
443 investigated further with climate analyses of long-term observations and a more comprehensive  
444 modeling of air quality and meteorology.

445 **Data availability:** Data used in this paper can be provided by Chao Yu (ychao012@foxmail.com)  
446 upon request.



447 **Author contributions:** CY, TZ and YB conducted the study design. XY, LZ and SK provided the  
448 observational data. LZ assisted with data processing. CY wrote the manuscript with the help of TZ  
449 and XY. YB, SK, JH, CC, YY, GM, MW and JC were involved in the scientific interpretation and  
450 discussion. All of the authors provided commentary on the paper.

451 **Competing interests:** The authors declare that they have no conflicts of interest.

452 **Acknowledgement:** This study was jointly funded by the National Natural Science Foundation of  
453 China (41830965; 91744209), the National Key R & D Program Pilot Projects of China  
454 (2016YFC0203304) and the Postgraduate Research & Practice Innovation Program of Jiangsu  
455 Province (KYCX18\_1027).

456

## 457 **Reference**

- 458 Acciai, C., Zhang, Z., Wang, F., Zhong, Z., and Lonati, G.: Characteristics and source Analysis of  
459 trace Elements in PM<sub>2.5</sub> in the Urban Atmosphere of Wuhan in Spring, Aerosol and Air Quality  
460 Research, 17, <https://doi.org/2224-2234>, 10.4209/aaqr.2017.06.0207, 2017.
- 461 An, X., Yao, B., Li, Y., Li, N., and Zhou, L.: Tracking source area of Shangdianzi station using  
462 Lagrangian particle dispersion model of FLEXPART, Meteorological Applications, 21, 466-473,  
463 <https://doi.org/10.1002/met.1358>, 2014.
- 464 An, Z., Huang, R.-J., Zhang, R., Tie, X., Li, G., Cao, J., Zhou, W., Shi, Z., Han, Y., and Gu, Z.:  
465 Severe haze in Northern China: A synergy of anthropogenic emissions and atmospheric processes,  
466 Proceedings of the National Academy of Sciences, 116, 8657-8666,  
467 <https://doi.org/10.1073/pnas.1900125116>, 2019.



468 Brioude, J., Arnold, D., Stohl, A., Cassiani, M., Morton, D., Seibert, P., Angevine, W., Evan, S.,  
469 Dingwell, A., Fast, J. D., Easter, R. C., Pissò, I., Burkhardt, J., and Wotawa, G.: The Lagrangian  
470 particle dispersion model FLEXPART-WRF version 3.1, *Geoscientific Model Development*, 6,  
471 1889-1904, <https://doi.org/10.5194/gmd-6-1889-2013>, 2013.

472 Cao, J. J., Wang, Q. Y., Chow, J. C., Watson, J. G., Tie, X. X., Shen, Z. X., Wang, P., and An, Z. s.:  
473 Impacts of aerosol compositions on visibility impairment in Xi'an, China, *Atmospheric*  
474 *Environment*, 59, 559-566, <https://doi.org/10.1016/j.atmosenv.2012.05.036>, 2012.

475 Chang, X., Wang, S., Zhao, B., Cai, S., and Hao, J.: Assessment of inter-city transport of  
476 particulate matter in the Beijing–Tianjin–Hebei region, *Atmospheric Chemistry and Physics*, 18,  
477 4843-4858, <https://doi.org/10.5194/acp-18-4843-2018>, 2018.

478 Chen, B., Xu, X.-D., and Zhao, T.: Quantifying oceanic moisture exports to mainland China in  
479 association with summer precipitation, *Climate Dynamics*, 1-16,  
480 <https://doi.org/10.1007/s00382-017-3925-1>, 2017a.

481 Chen, S., Zhou, G., Zhu, B., Geng, F., and Chang, L.: A method for fast quantification of air  
482 pollutant sources, *Acta Scientiae Circumstantiae*, 2474-2481, 2017b.

483 Cheng, Y. F., Wiedensohler, A., Eichler, H., Heintzenberg, J., Tesche, M., Ansmann, A., Wendisch,  
484 M., Su, H., Althausen, D., and Herrmann, H.: Relative humidity dependence of aerosol optical  
485 properties and direct radiative forcing in the surface boundary layer at Xinken in Pearl River Delta  
486 of China: An observation based numerical study, *Atmospheric Environment*, 42, 6373-6397,  
487 <https://doi.org/10.1016/j.atmosenv.2008.04.009>, 2008.

488 De Foy, B., Burton, S. P., Ferrare, R. A., Hostetler, C. A., Hair, J. W., Wiedinmyer, C., and Molina,  
489 L. T.: Aerosol plume transport and transformation in high spectral resolution lidar measurements



490 and WRF-Flexpart simulations during the MILAGRO Field Campaign, Atmospheric Chemistry  
491 and Physics, 11, 3543-3563, <https://doi.org/10.5194/acp-11-3543-2011>, 2011.

492 Deng, J., Wang, T., Jiang, Z., Xie, M., Zhang, R., Huang, X., and Zhu, J.: Characterization of  
493 visibility and its affecting factors over Nanjing, China, Atmospheric Research, 101, 681-691,  
494 <https://doi.org/10.1016/j.atmosres.2011.04.016>, 2011.

495 Ding, Y. H.: Monsoons over China, Kluwer Academic Publishers, Dordrecht/Boston/London,  
496 1994.

497 Ding, Y., Wu, P., Liu, Y., and Song, Y.: Environmental and dynamic conditions for the occurrence  
498 of persistent haze events in north China, Engineering, 3, 266-271, 2017.

499 Fast, J. D., and Easter, R. C.: A Lagrangian particle dispersion model compatible with WRF, 7th  
500 Annual WRF User's Workshop, 2006, 19-22.

501 Fuzzi, S., Baltensperger, U., Carslaw, K., Decesari, S., Denier van der Gon, H., Facchini, M. C.,  
502 Fowler, D., Koren, I., Langford, B., and Lohmann, U.: Particulate matter, air quality and climate:  
503 lessons learned and future needs, Atmospheric chemistry and physics, 15, 8217-8299,  
504 <https://doi.org/10.5194/acp-15-8217-2015>, 2015.

505 Gong, W., Zhang, T., Zhu, Z., Ma, Y., Ma, X., and Wang, W.: Characteristics of PM<sub>1.0</sub>, PM<sub>2.5</sub>,  
506 and PM<sub>10</sub>, and Their Relation to Black Carbon in Wuhan, Central China, Atmosphere, 6,  
507 1377-1387, <https://doi.org/10.3390/atmos6091377>, 2015.

508 Grell, G. A., Peckham, S. E., Schmitz, R., McKeen, S. A., Frost, G., Skamarock, W. C., & Eder,  
509 B. . Fully coupled 'online' chemistry within the WRF model. Atmospheric Environment,  
510 39(37):6957-6975, <https://doi.org/10.1016/j.atmosenv.2005.04.027>, 2005.

511 He, J., Mao, H., Gong, S., Yu, Y., Wu, L., Liu, H., Chen, Y., Jing, B., Ren, P., and Zou, C.:





Investigation of Particulate Matter Regional Transport in Beijing Based on Numerical Simulation,  
Aerosol and Air Quality Research, 17, 1181-1189, <https://doi.org/10.4209/aaqr.2016.03.0110>,  
2017.

Hong S Y, Noh Y, Dudhia J. : A new vertical diffusion package with an explicit treatment of  
entrainment processes, Monthly Weather Review, 134, 2318-2341,  
<https://doi.org/10.1175/MWR3199.1.2006>.

Hu, J., Li, Y., Zhao, T., Liu, J., Hu, X.-M., Liu, D., Jiang, Y., Xu, J., and Chang, L.: An important  
mechanism of regional O<sub>3</sub> transport for summer smog over the Yangtze River Delta in eastern  
China, Atmospheric Chemistry and Physics, 18, 16239-16251,  
<https://doi.org/10.5194/acp-18-16239-2018>, 2018.

Huang, Q., Cai, X., Wang, J., Song, Y., and Zhu, T.: Climatological study of the Boundary-layer  
air Stagnation Index for China and its relationship with air pollution, Atmos. Chem. Phys., 18,  
7573–7593, <https://doi.org/10.5194/acp-18-7573-2018>, 2018.

Jiang, C., Wang, H., Zhao, T., Li, T., and Che, H.: Modeling study of PM<sub>2.5</sub> pollutant transport  
across cities in China's Jing–Jin–Ji region during a severe haze episode in December 2013,  
Atmospheric Chemistry and Physics, 15, 5803-5814, <https://doi.org/10.5194/acp-15-5803-2015>,  
2015.

Kan, H., Chen, R., and Tong, S.: Ambient air pollution, climate change, and population health in  
China, Environment international, 42, 10-19, <https://doi.org/10.1016/j.envint.2011.03.003>, 2012.

Kang, H., Zhu, B., Gao, J., He, Y., Wang, H., Su, J., Pan, C., Zhu, T., and Yu, B.: Potential impacts  
of cold frontal passage on air quality over the Yangtze River Delta, China, Atmospheric Chemistry  
and Physics, 19, 3673-3685, <https://doi.org/10.5194/acp-19-3673-2019>, 2019.



534 Miao, Y., Guo, J., Liu, S., Zhao, C., Li, X., Zhang, G., Wei, W., and Ma, Y.: Impacts of synoptic  
535 condition and planetary boundary layer structure on the trans-boundary aerosol transport from  
536 Beijing-Tianjin-Hebei region to northeast China, *Atmospheric Environment*, 181, 1-11,  
537 <https://doi.org/10.1016/j.atmosenv.2018.03.005>, 2018.

538 Mlawer, E. J., Taubman, S. J., Brown, P. D., Iacono, M. J., and Clough, S. A.: Radiative transfer  
539 for inhomogeneous atmospheres: RRTM, a validated correlated-k model for the longwave, *Journal*  
540 *of Geophysical Research: Atmospheres*, 102, 16663-16682, <https://doi.org/10.1029/97jd00237>,  
541 1997.

542 Morrison, H.: Impact of cloud microphysics on the development of trailing stratiform precipitation  
543 in a simulated squall line: Comparison of one-and two-moment schemes, *Mon. wea. rev.*, 137,  
544 991-1007, <https://doi.org/10.1175/2008MWR2556.1>, 2009.

545 Nel, A.: Air pollution-related illness: effects of particles, *Science*, 308, 804-806,  
546 <https://doi.org/10.1126/science.1108752>, 2005.

547 Oke, T. R.: *Boundary layer climates*, Routledge, 2002.

548 Qiao, X., Guo, H., Tang, Y., Wang, P., Deng, W., Zhao, X., Hu, J., Ying, Q., and Zhang, H.: Local  
549 and regional contributions to fine particulate matter in the 18 cities of Sichuan Basin, southwestern  
550 China, *Atmos. Chem. Phys.*, 19, 5791–5803, <https://doi.org/10.5194/acp-19-5791-2019>, 2019.

551 Sauvage, B., Fontaine, A., Eckhardt, S., Aubry, A., Boulanger, D., Petetin, H., Paugam, R., Athier,  
552 G., Cousin, J.-M., Darras, S., Nédélec, P., Stohl, A., Turquety, S., Cammas, J.-P., and Thouret, V.:  
553 Source attribution using FLEXPART and carbon monoxide emission inventories: SOFT-IO  
554 version 1.0, *Atmospheric Chemistry and Physics*, 17, 15271-15292,  
555 <https://doi.org/10.5194/acp-17-15271-2017>, 2017.



556 Seibert, P., and Frank, A.: Source-receptor matrix calculation with a Lagrangian particle dispersion  
557 model in backward mode, *Atmospheric Chemistry and Physics*, 51-63,  
558 <https://doi.org/10.5194/acp-4-51-2004>, 2003.

559 Sheng, P., Mao, J., and Li, J.: *Atmospheric physics*, Peking University Press, 2003.

560 Stohl, A.: A backward modeling study of intercontinental pollution transport using aircraft  
561 measurements, *Journal of Geophysical Research*, 108, 1-8, <https://doi.org/10.1029/2002jd002862>,  
562 2003.

563 Tan, C. H., Zhao, T. L., Cui, C. G., Luo, B. L., Zhang, L., and Bai, Y. Q.: Characterization of haze  
564 pollution over Central China during the past 50 years, *China Environmental Science*, 35,  
565 2272-2280, 2015.

566 Taylor, K. E.: Summarizing multiple aspects of model performance in a single diagram, *Journal of*  
567 *Geophysical Research Atmospheres*, 106, 7183-7192, <https://doi.org/10.1029/2000JD900719>,  
568 2001.

569 Tie, X., Huang, R. J., Cao, J., Zhang, Q., Cheng, Y., Su, H., Chang, D., Poschl, U., Hoffmann, T.,  
570 Dusek, U., Li, G., Worsnop, D. R., and O'Dowd, C. D.: Severe Pollution in China Amplified by  
571 Atmospheric Moisture, *Scientific reports*, 7, 1-8, <https://doi.org/10.1038/s41598-017-15909-1>,  
572 2017.

573 Wang, H. L., Qiao, L. P., Lou, S. R., Zhou, M., Ding, A. J., Huang, H. Y., Chen, J. M., Wang, Q.,  
574 Tao, S. K., Chen, C. H., Li, L., and Huang, C.: Chemical composition of PM<sub>2.5</sub> and  
575 meteorological impact among three years in urban Shanghai, China, *Journal of Cleaner Production*,  
576 112, 1302-1311, <https://doi.org/10.1016/j.jclepro.2015.04.099>, 2016.

577 Wang, S. X., Zhao, B., Cai, S. Y., Klimont, Z., Nielsen, C. P., Morikawa, T., Woo, J. H., Kim, Y.,



578 Fu, X., Xu, J. Y., Hao, J. M., and He, K. B.: Emission trends and mitigation options for air  
579 pollutants in East Asia, *Atmospheric Chemistry and Physics*, 14, 6571-6603,  
580 <https://doi.org/10.5194/acp-14-6571-2014>, 2014.

581 Wu, J., Kong, S., Wu, F., Cheng, Y., Zheng, S., Yan, Q., Zheng, H., Yang, G., Zheng, M., and Liu,  
582 D.: Estimating the open biomass burning emissions in central and eastern China from 2003 to  
583 2015 based on satellite observation, *Atmospheric Chemistry & Physics*, 18,  
584 <https://doi.org/10.5194/acp-18-11623-2018>, 2018.

585 Wu, P., Ding, Y., and Liu, Y.: Atmospheric Circulation and Dynamic Mechanism for Persistent  
586 Haze Events in the Beijing-Tianjin-Hebei Region, *Advances in Atmospheric Sciences*, 34,  
587 429-440, 2017.

588 Xu, G., Jiao, L., Zhang, B., Zhao, S., Yuan, M., Gu, Y., Liu, J., and Tang, X.: Spatial and Temporal  
589 Variability of the PM<sub>2.5</sub>/PM<sub>10</sub> Ratio in Wuhan, Central China, *Aerosol and Air Quality Research*,  
590 17, 741-751, <https://doi.org/10.4209/aaqr.2016.09.0406>, 2017.

591 Xu, J., Chang, L., Qu, Y., Yan, F., Wang, F., and Fu, Q.: The meteorological modulation on PM<sub>2.5</sub>  
592 interannual oscillation during 2013 to 2015 in Shanghai, China, *Science of The Total Environment*,  
593 572, 1138-1149, <https://doi.org/10.1016/j.scitotenv.2016.08.024>, 2016a.

594 Xu, X., Zhao, T., Liu, F., Gong, S. L., Kristovich, D., Lu, C., Guo, Y., Cheng, X., Wang, Y., and  
595 Ding, G.: Climate modulation of the Tibetan Plateau on haze in China, *Atmospheric Chemistry  
596 and Physics*, 16, 1365-1375, <https://doi.org/10.5194/acp-16-1365-2016>, 2016b.

597 Zhai, S., An, X., Liu, Z., Sun, Z., and Hou, Q.: Model assessment of atmospheric pollution control  
598 schemes for critical emission regions, *Atmospheric Environment*, 124, 367-377,  
599 <https://doi.org/10.1016/j.atmosenv.2015.08.093>, 2016.



600 Zhang, F., Wang, Z.-w., Cheng, H.-r., Lv, X.-p., Gong, W., Wang, X.-m., and Zhang, G.: Seasonal  
601 variations and chemical characteristics of PM<sub>2.5</sub> in Wuhan, central China, *Science of the Total*  
602 *Environment*, 518, 97-105, <https://doi.org/10.1016/j.scitotenv.2015.02.054>, 2015.

603 Zhang, H., Lv, M., and Zhang, B.: Analysis of the stagnant meteorological situation and the  
604 transmission condition of continuous heavy pollution course from February 20 to 26, 2014 in  
605 Beijing-Tianjin-Hebei, *Acta Scientiae Circumstantiae* 36, 4340-4351, 2016.

606 Zhang, R., Li, Q., and Zhang, R.: Meteorological conditions for the persistent severe fog and haze  
607 event over eastern China in January 2013, *Science China Earth Sciences*, 57, 26-35,  
608 <https://doi.org/10.1007/s11430-013-4774-3>, 2014.

609 Zhang, X. Y., Wang, Y. Q., Niu, T., Zhang, X. C., Gong, S. L., Zhang, Y. M., and Sun, J. Y.:  
610 Atmospheric aerosol compositions in China: spatial/temporal variability, chemical signature,  
611 regional haze distribution and comparisons with global aerosols, *Atmospheric Chemistry and*  
612 *Physics*, 12, 779-799, <https://doi.org/10.5194/acp-12-779-2012>, 2012.

613 Zheng, H., Kong, S., Wu, F., Cheng, Y., Niu, Z., Zheng, S., Yang, G., Yao, L., Yan, Q., and Wu, J.:  
614 Intra-regional transport of black carbon between the south edge of the North China Plain and  
615 central China during winter haze episodes, *Atmospheric Chemistry and Physics*, 19, 4499-4516,  
616 <https://doi.org/10.5194/acp-19-4499-2019>, 2019.

617 Zhong, Zhangxiong, Huang, Zhen, Ting, Shen, and Longjiao: Characteristic Analysis of OC and  
618 EC in PM<sub>2.5</sub> of Typical Haze Weather in Wuhan City, *Meteorological and Environmental*  
619 *Research*, 19-22, 2014.

620

621



622

623

624

625 **Table 1.** Correlation coefficients between hourly  $PM_{2.5}$  concentrations and meteorological  
 626 elements over Wuhan in January 2016.

Correlation coefficient	WS	T	P	RH
$PM_{2.5}$	0.10	0.31	-0.47	0.20

627

628 **Table 2.** Correlation coefficients of  $PM_{2.5}$  concentrations with wind speed and air temperature in  
 629 different air quality levels during the study period.

Air quality	$PM_{2.5}$ levels	Number of samples	WS	T
Clean	$PM_{2.5} < 75 \mu g \cdot m^{-3}$	73	-0.20	0.56
Light pollution	$75 \mu g \cdot m^{-3} \leq PM_{2.5} < 150 \mu g \cdot m^{-3}$	135	-0.19	0.15
Heavy pollution	$PM_{2.5} \geq 150 \mu g \cdot m^{-3}$	37	0.41	-0.08

630



631

632

633

634 **Table 3.** Atmospheric static stability below heights of 200 m in the boundary layer during heavy  
 635 pollution and clean air periods with the anomalies relative to the average over January, 2016 in  
 636 Wuhan.

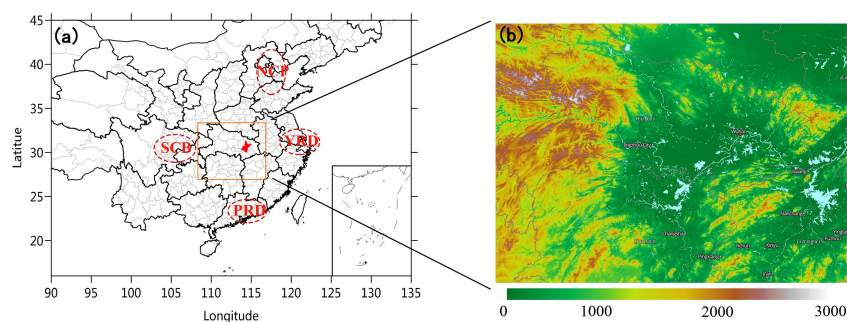
Period	heavy pollution period	clean air period	monthly average
	(K·km-1)	(K·km-1)	(K·km-1)
Static stability	4.4	13.2	8.6
Anomalies of stability	-4.2	4.6	-

637

638 **Table 4.** The relative contributions of regional transport over central-eastern China to three PM<sub>2.5</sub>  
 639 heavy pollution periods P1, P2 and P3 in the YRMB with the local contributions.

Contribution rates	P1	P2	P3	Averages
Regional transport	68.1%	60.9%	65.3%	65.1%
Local contribution	31.9%	39.1%	34.7%	34.9%

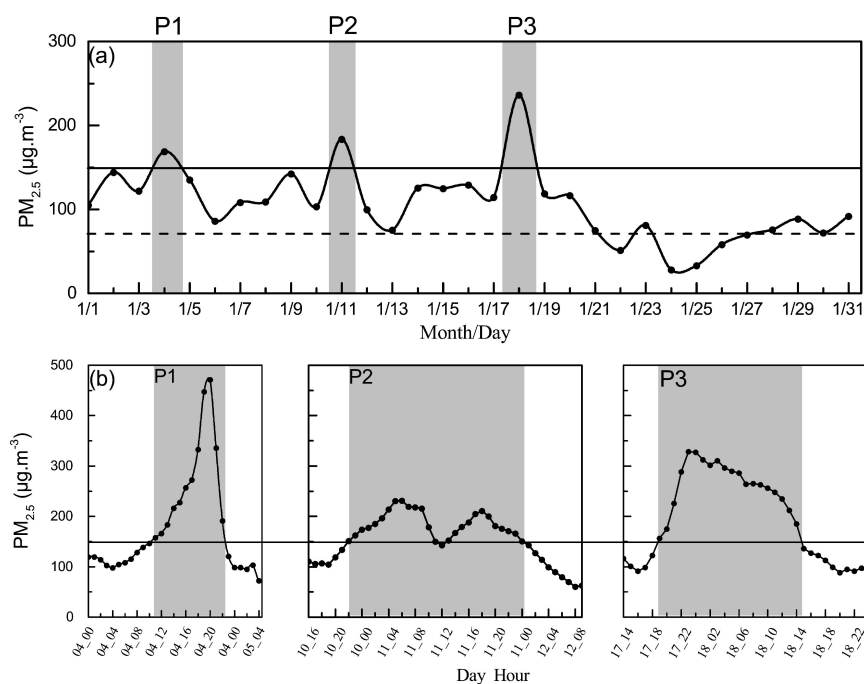
640



641

642 **Fig. 1.** (a) Distribution of the Yangtze River Middle Basin (orange rectangle) with the location of  
 643 Wuhan (red area) and the major haze pollution regions of NCP, YPD and SCB in central-eastern  
 644 China as well as (b) the YRMB region with terrain height (color contours, m in a.s.l.), the rivers  
 645 and lake network (blue areas), downloaded from <https://worldview.earthdata.nasa.gov>.

646



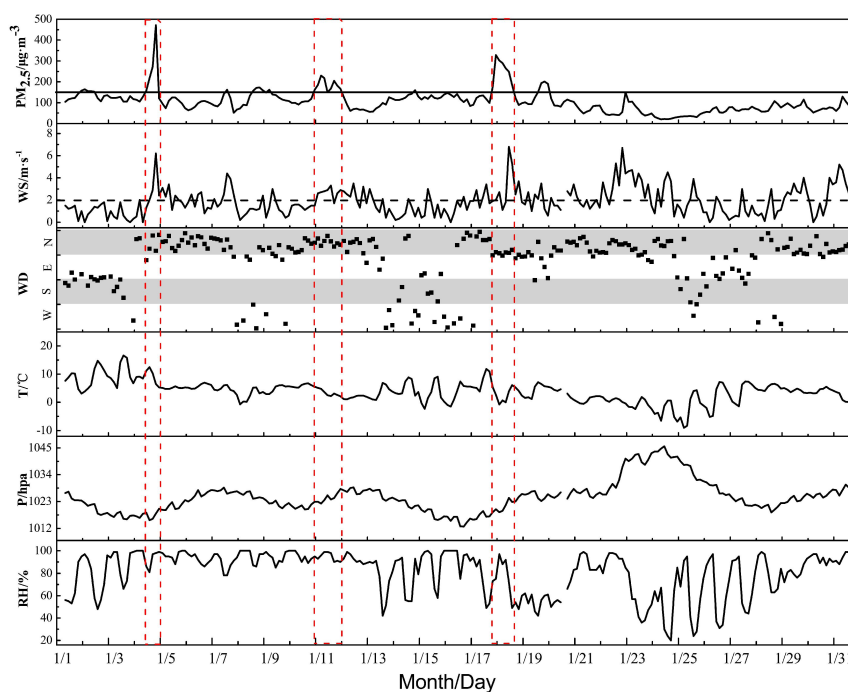
647





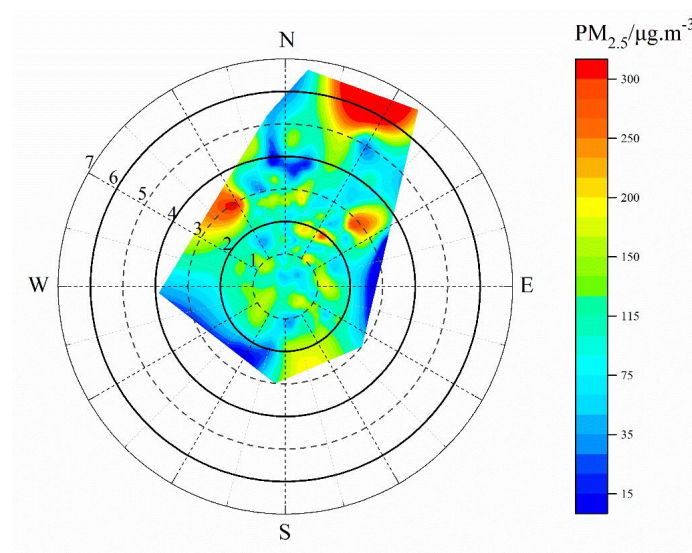
648 **Fig. 2.** (a) The daily changes of surface  $\text{PM}_{2.5}$  concentrations in Wuhan in January 2016 with  
 649  $\text{PM}_{2.5}$  concentrations exceeding  $75 \mu\text{g}\cdot\text{m}^{-3}$  (dash line) and  $150 \mu\text{g}\cdot\text{m}^{-3}$  (solid lines), respectively,  
 650 for light and heavy haze pollution, and (b) the hourly variation of surface  $\text{PM}_{2.5}$  concentrations in  
 651 three heavy air pollution events P1, P2 and P3 with excessive  $\text{PM}_{2.5}$  levels ( $>150 \mu\text{g}\cdot\text{m}^{-3}$ ) marked  
 652 by the shaded areas.

653



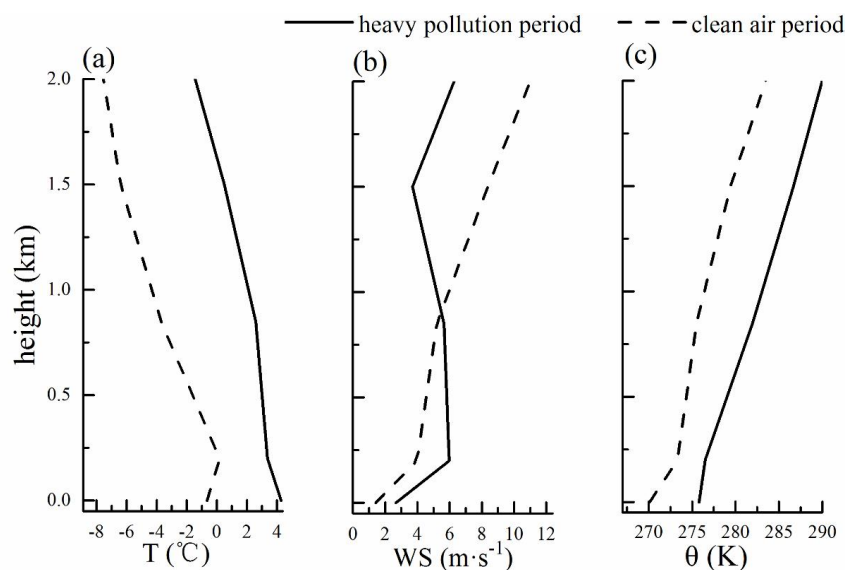
654

655 **Fig. 3.** Hourly variations of meteorological elements and  $\text{PM}_{2.5}$  concentrations in Wuhan in  
 656 January 2016 with heavy air pollution periods marked with the columns in red dash lines and  
 657  $\text{PM}_{2.5}$  concentrations exceeding  $150 \mu\text{g}\cdot\text{m}^{-3}$  (solid line).



658

659 **Fig. 4.** A polar plot of hourly variations in wind speed (round radius, units is  $\text{m}\cdot\text{s}^{-1}$ ) and direction  
 660 (angles) to surface  $\text{PM}_{2.5}$  concentrations (color contours, units is  $\mu\text{g}\cdot\text{m}^{-3}$ ) in Wuhan in January,  
 661 2016.

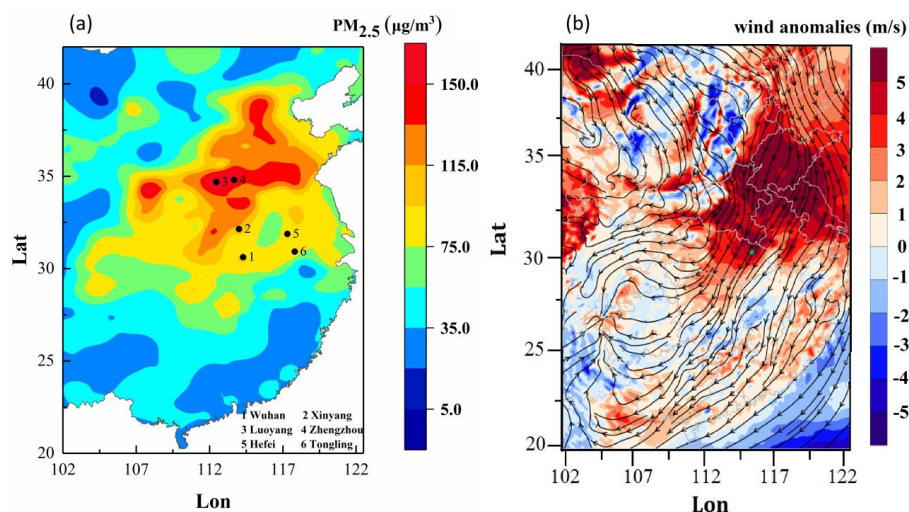


662

663 **Fig. 5.** Vertical profiles of (a) air temperature, (b) wind velocity and (c) potential temperature



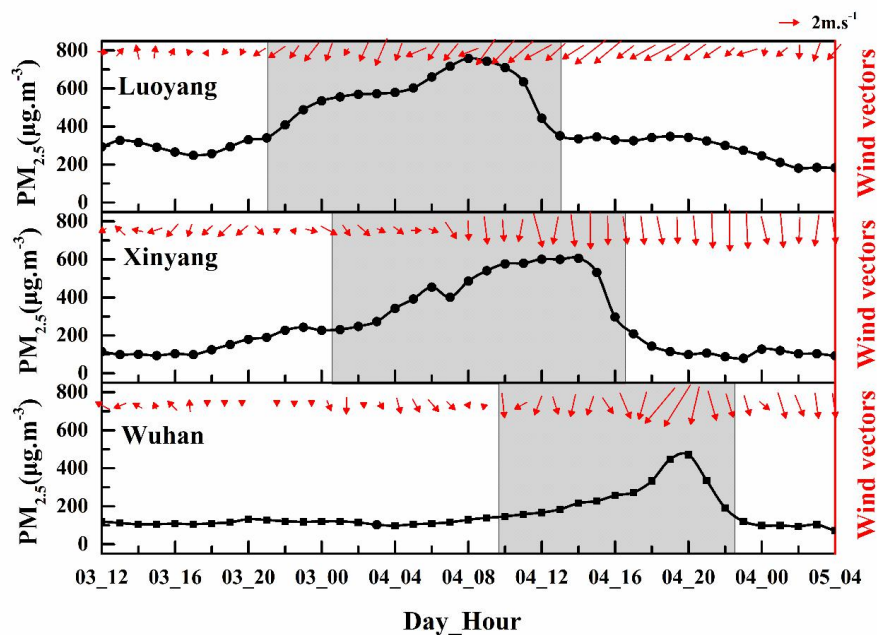
664 averaged in heavy  $\text{PM}_{2.5}$  pollution and clean air periods over Wuhan during January 2016.



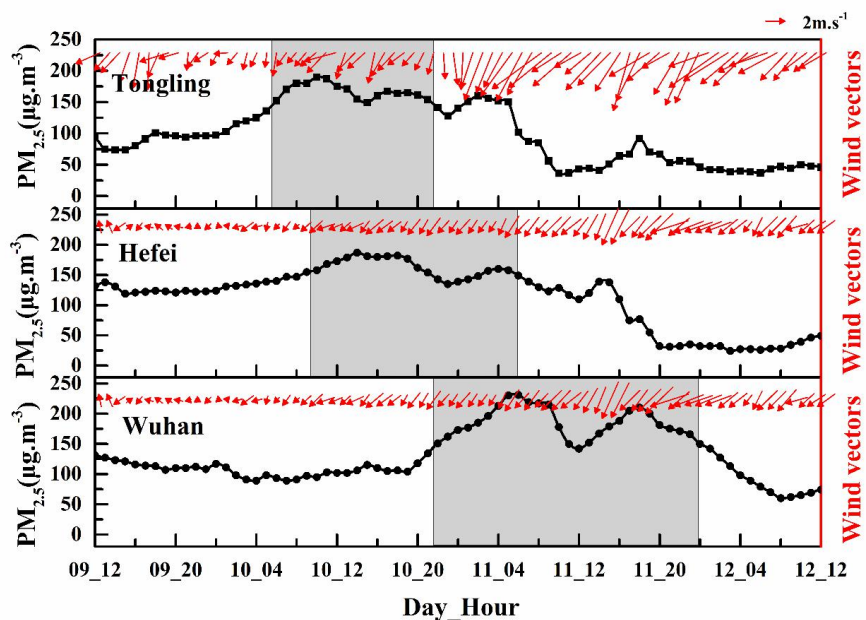
665

666 **Fig. 6** Distribution of (a) monthly averages of surface  $\text{PM}_{2.5}$  concentrations observed in January  
 667 2016 over central-eastern regions in mainland China with the locations of six sites 1. Wuhan, 2.  
 668 Xinyang, 3. Luoyang, 4. Zhengzhou, 5. Hefei and 6. Tongling as well as (b) the anomalies (color  
 669 contours) of 200m wind speeds averaged during three heavy air pollution periods relatively to the  
 670 monthly wind averages (streamlines) in January 2016 over central-eastern China with the location  
 671 of Wuhan (a light blue star).

672

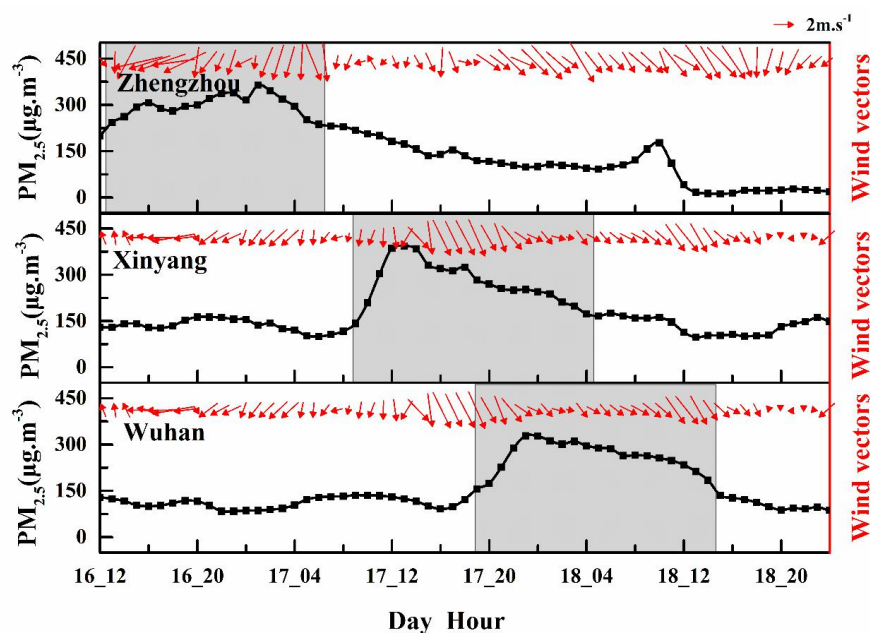


673



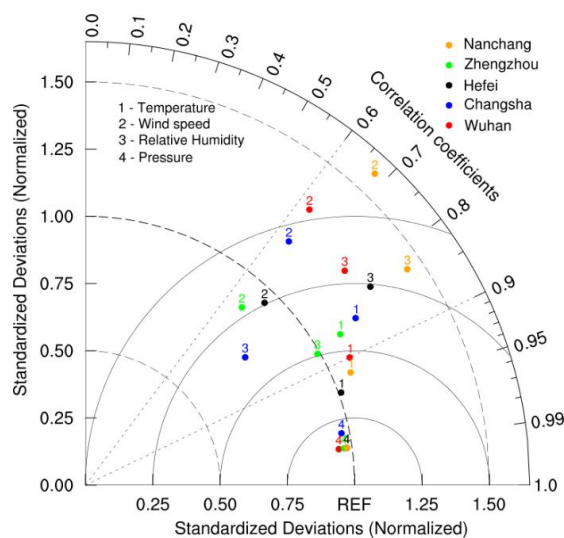
674

675



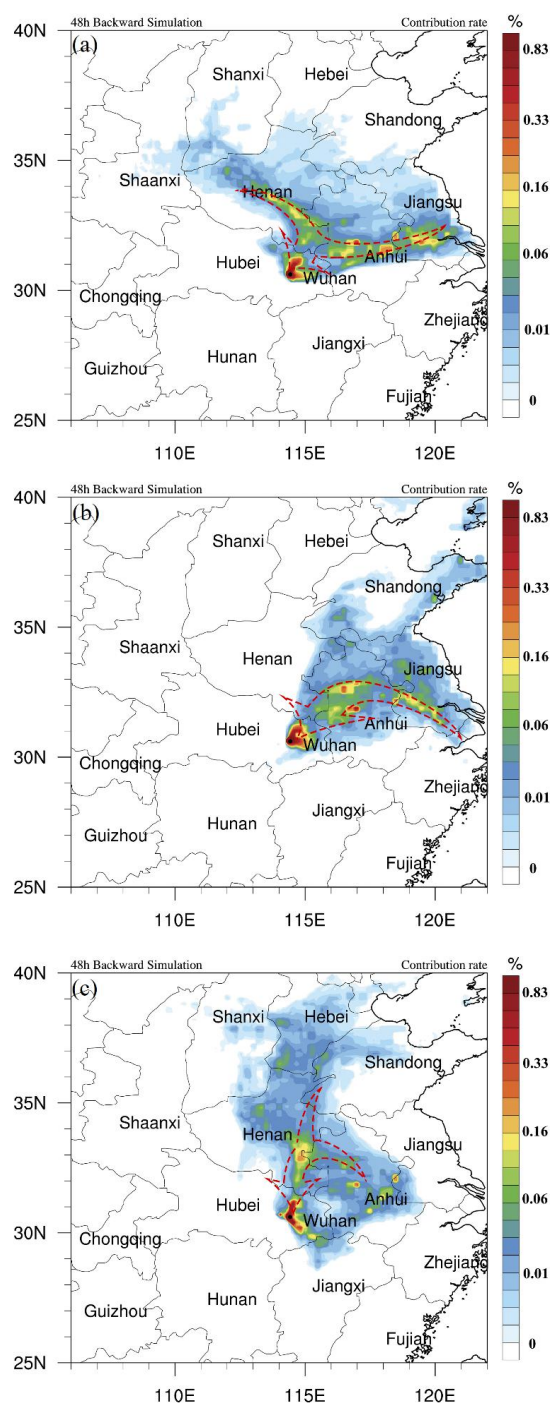
676  
 677 **Fig. 7.** Temporal changes of  $PM_{2.5}$  concentrations (dot lines) and near-surface winds (vectors)  
 678 observed at five upstream sites (Fig. 6) and Wuhan with shifts of  $PM_{2.5}$  peaks (marked with shaded  
 679 areas) to the YRMB's heavy  $PM_{2.5}$  pollution periods P1 P2 and P3 (respectively in upper, middle  
 680 and lower panels) in January 2016.

681



682

683 **Fig. 8.** Taylor plots with the normalized standard deviations and correlation coefficients between  
 684 simulated and observed meteorological fields. The radian of the sector represents the correlation  
 685 coefficient, the solid line indicates the ratio of standard deviation between simulations and  
 686 observations, the distance from the marker to “REF” reflect the normalized root-mean-square error  
 687 (NRMSE).



688

689 **Fig. 9.** Spatial distribution of contribution rates (color contours) to  $PM_{2.5}$  concentrations in Wuhan





690 with the major pathways of regional transport over central-eastern China (dash arrows) for (a)  
691 heavy pollution periods P1, (b) P2 and (c) P3 in January, 2016 simulated by the model  
692 FLEXPART-WRF.

693